Surface wave tomography for geodynamically relevant anisotropic models

Mark Panning[1] and Guust Nolet[1,2]

1. Princeton University, 2. Now at Université Nice Sophia Antipolis

S23B-1372 - contact: mpanning@princeton.edu

Abstract

Using seismic data to constrain not only the strength of anisotropy, but the orientation of the best-fitting symmetry axis is important for geodynamic understanding, as this can be related to mantle convection flow patterns. Surface wave models, though, often only deal with anisotropy with a vertical axis of symmetry. Conversely, SKS splitting measurements have typically been modeled assuming a horizontal axis of symmetry for the material properties. Recently, however, methods have been developed for using splitting measurements in tomographic inversions for more general symmetry axis orientations (e.g. Chevrot 2006; Abt and Fischer 2007). There have also been surface wave studies which model azimuthal dependence of Rayleigh wave velocity through linearized dependence on a horizontal fast axis (e.g. Simons et al. 2002). As the frequency content of body wave splitting measurements and surface wave observations differ greatly, it is essential to have an appropriate finite frequency theory in order to include both in a consistent framework. We derive here nonlinear expressions for 3D finite-frequency surface wave sensitivity to arbitrarily oriented hexagonal symmetric media. We also discuss practical means of inverting for such a model, including combination with the compatible approach of shear wave splitting tomography proposed by Chevrot (2006).

Motivation

Anisotropic mantle velocity models, if sufficiently resolved, can be directly related to mantle convective flow patterns. Theoretical studies of predicted anisotropy due to mantle flow based on kinematic theory (e.g. Becker et al., 2006) suggest that at least upper mantle anisotropy may be well modeled using an anisotropic material with hexagonal symmetry, with the fast axis oriented roughly parallel with the long axis of the finite strain ellipse. Detailed anisotropic modeling may be compared with mantle flow calculations (e.g. figure 1) in order to better constrain the dynamics of the mantle. It is valuable then to attempt to directly resolve both strength and orientation of anisotropy.

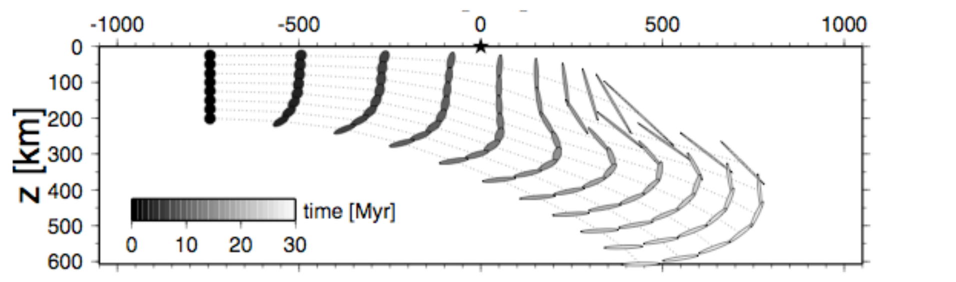

Figure1: Calculated finite strain ellipses for a flow field in the South American subduction zone (**from Becker et al., 2003**)

Theory

We wish to develop the surface wave sensitivity to an arbitrarily oriented hexagonal medium, as defined by Chevrot (2006)

$$\begin{aligned}\delta c_{ijkl} &= \delta\lambda\delta_{ij}\delta_{kl} + \delta\mu(\delta_{ik}\delta_{jl} + \delta_{il}\delta_{jk})\\ &+ 2\rho\alpha^2\epsilon(\hat{s}_i\hat{s}_j\hat{s}_k\hat{s}_l - \delta_{ij}\hat{s}_k\hat{s}_l - \delta_{kl}\hat{s}_i\hat{s}_j)\\ &+ \rho\alpha^2\delta(\delta_{ij}\hat{s}_k\hat{s}_l + \delta_{kl}\hat{s}_i\hat{s}_j - 2\hat{s}_i\hat{s}_j\hat{s}_k\hat{s}_l)\\ &+ 2\rho\beta^2\gamma(2\delta_{ij}\hat{s}_k\hat{s}_l + 2\delta_{kl}\hat{s}_i\hat{s}_j - \delta_{il}\hat{s}_j\hat{s}_k - \delta_{jk}\hat{s}_i\hat{s}_l - \delta_{jl}\hat{s}_i\hat{s}_k - \delta_{ik}\hat{s}_j\hat{s}_l)\end{aligned}$$

where the elastic properties are described by perturbations to the isotropic Lame parameters, λ and μ, and the three anisotropic parameters ε, δ, and γ (Mensch and Rasolofosaon 1997), defined by elements of a Voigt matrix relative to the symmetry axis $\hat{s}$ (figure 2) as

$$\begin{aligned}\epsilon &= (C_{11} - C_{33})/2(\lambda + 2\mu)\\ \delta &= (C_{13} - C_{33} + 2C_{44})/(\lambda + 2\mu)\\ \gamma &= (C_{66} - C_{44})/2\mu\\ \delta\lambda &= C_{11} - 2C_{66} - \lambda\\ \delta\mu &= C_{66} - \mu.\end{aligned}$$

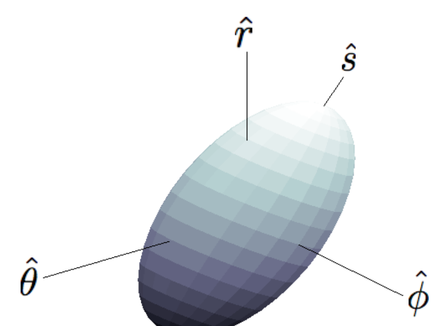

Figure 2: Representation of hexagonal symmetry with axis specified by $\hat{s}$.

We define the Green tensor of a surface wave at a specific frequency as

$$\mathbf{G}^{rs} = \mathbf{p}_r\mathbf{p}_s^* P(\theta)$$

where **p** is a polarization vector and P is a propagation term

$$\mathbf{p} = U(r)\hat{r} - iV(r)\hat{\theta} + iW(r)\hat{\phi} \qquad P(\theta) = \frac{e^{-i(\nu\theta + \pi/4 - n\pi/2)}}{|8\pi\nu\sin\theta|^{\frac{1}{2}}}$$

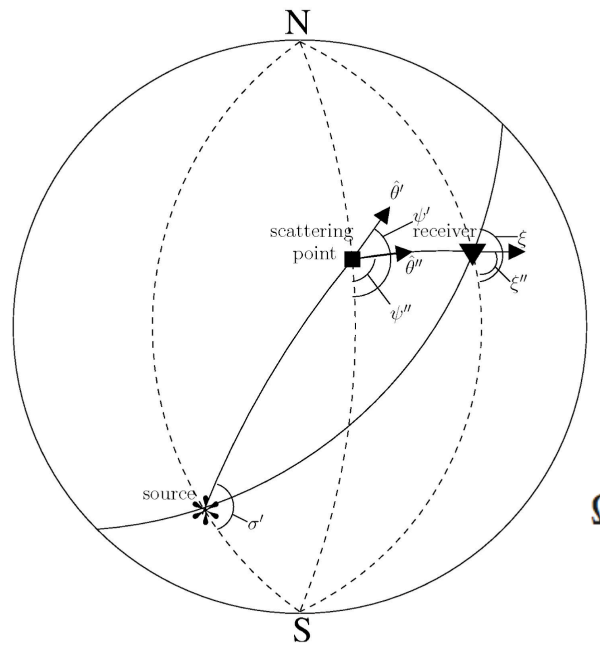

Figure 3: Cartoon depicting geometry of source, receiver and scattering point.

With that, we can define the first order Born approximation to the perturbed Green tensor as an integral over scattering points

$$\delta G_{il}^{rs} = -\int \partial_m G_{ij}^{rx}\delta c_{jmnk}\partial_n G_{kl}^{xs} d^3\vec{x}$$

and putting in the surface wave Green tensor, we get

$$\delta u_i = \delta G_{il}^{rs} = -\int p_{ri}P(\theta'')P(\theta')p_{sl}^*\Omega_X d^3\vec{x}$$

The interaction coefficient matrix is defined by

$$\Omega_X = [\partial_m p_{xj}''^* + i\nu'' r^{-1}\hat{\theta}_m'' p_{xj}''^*][\partial_n p_{xk}' - i\nu' r^{-1}\hat{\theta}_n' p_{xk}']\delta c_{jmnk}$$

where the ´ and ˝ refer to the incoming and outgoing wave respectively at the scattering point (figure 3). Each element of this matrix represents a coupling between modes defined by their eigenvectors and the orientation of the axis $\hat{s}$.

This can be modified for an expression for a perturbed moment tensor response using the S and R terms from Zhou et al. (2004) to

$$\delta s = -\int \mathcal{S}'\mathcal{R}'' P(\theta'')P(\theta')\Omega_X d^3\vec{x}$$

Assembling waveform sensitivity kernels

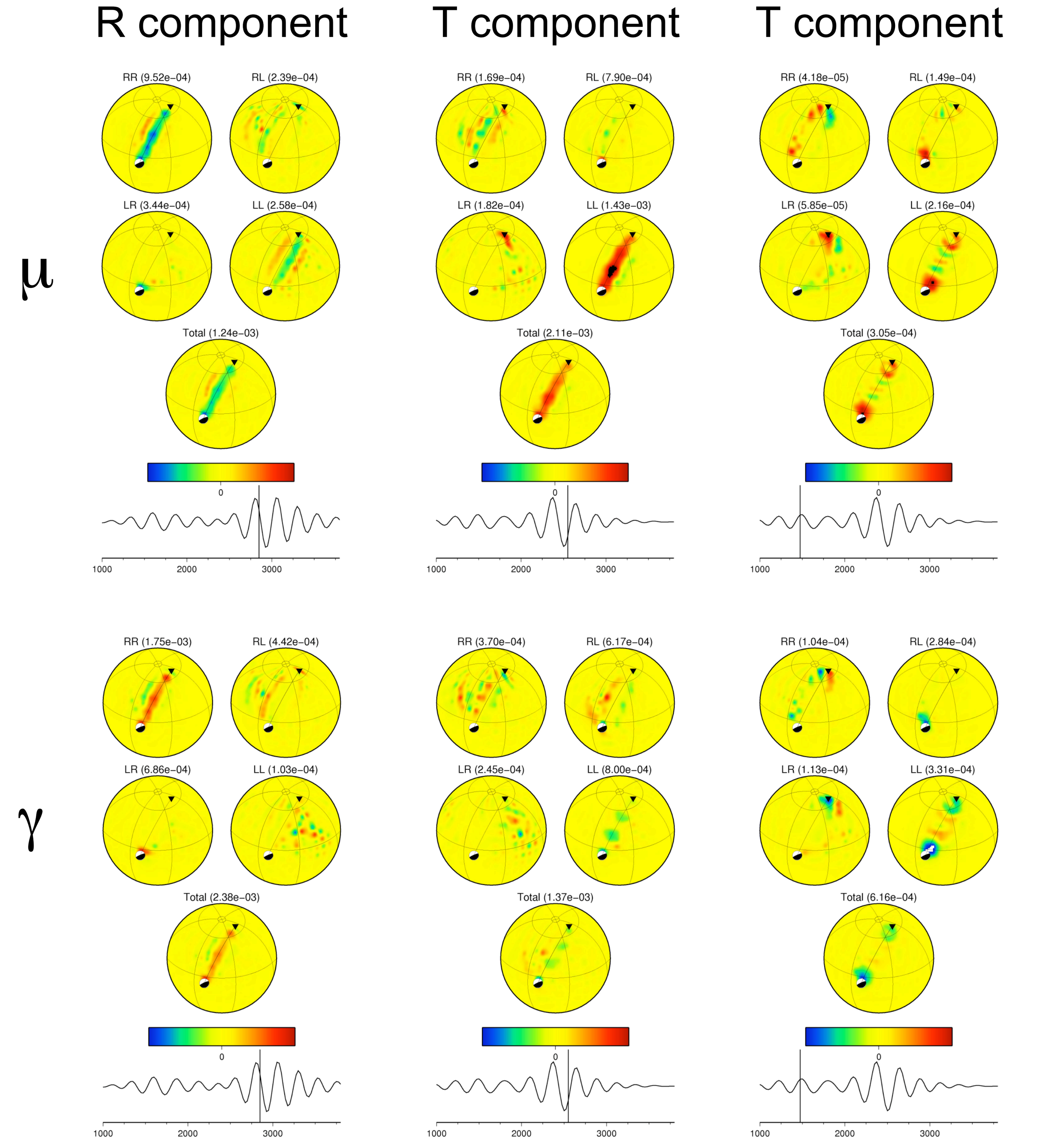

Figure 4: Contributions of different coupling of Rayleigh (R) and Love (L) to μ kernels (top) and kernels for γ (bottom) for a long period fundamental Rayleigh wave (left), fundamental Love wave (middle) and Love overtones (right). All slices are at 200 km depth, and data is filtered between 250 and 1000 seconds.

We show examples of waveform kernels calculated for long period surface waves with the same source-receiver configuration (figure 4). For greater physical intuition of the significance of the geographic patterns, we also show the components of the kernel due to coupling of fundamental and higher Rayleigh modes (RR), Rayleigh to Love (RL) and Love to Rayleigh conversions (LR), and coupling between fundamental and higher Love modes (LL). While relatively simple kernels emerge for μ during both the Rayleigh and Love fundamental modes, as well as the shear velocity anisotropic parameter γ in the fundamental Rayleigh wave, greater complexity and importance of mode conversions can be seen in the other kernels. These kernels are calculated for an initial model with a vertical axis of symmetry.

Nonlinearity

Because the elements of Ω for the anisotropic parameters ε, δ, and γ depend on the orientation of the symmetry axis in the starting model (figure 5), the problem is non-linear. We can define the kernels for perturbations to the orientation angles for an iterative inversion as

$$\frac{\partial u_i}{\partial\theta_s} = \epsilon\left(\frac{\partial K_\epsilon}{\partial s_j}\right)\left(\frac{\partial s_j}{\partial\theta_s}\right) + \delta\left(\frac{\partial K_\delta}{\partial s_j}\right)\left(\frac{\partial s_j}{\partial\theta_s}\right) + \gamma\left(\frac{\partial K_\gamma}{\partial s_j}\right)\left(\frac{\partial s_j}{\partial\theta_s}\right)$$

$$\frac{\partial u_i}{\partial\phi_s} = \epsilon\left(\frac{\partial K_\epsilon}{\partial s_j}\right)\left(\frac{\partial s_j}{\partial\phi_s}\right) + \delta\left(\frac{\partial K_\delta}{\partial s_j}\right)\left(\frac{\partial s_j}{\partial\theta_s}\right) + \gamma\left(\frac{\partial K_\gamma}{\partial s_j}\right)\left(\frac{\partial s_j}{\partial\phi_s}\right)$$

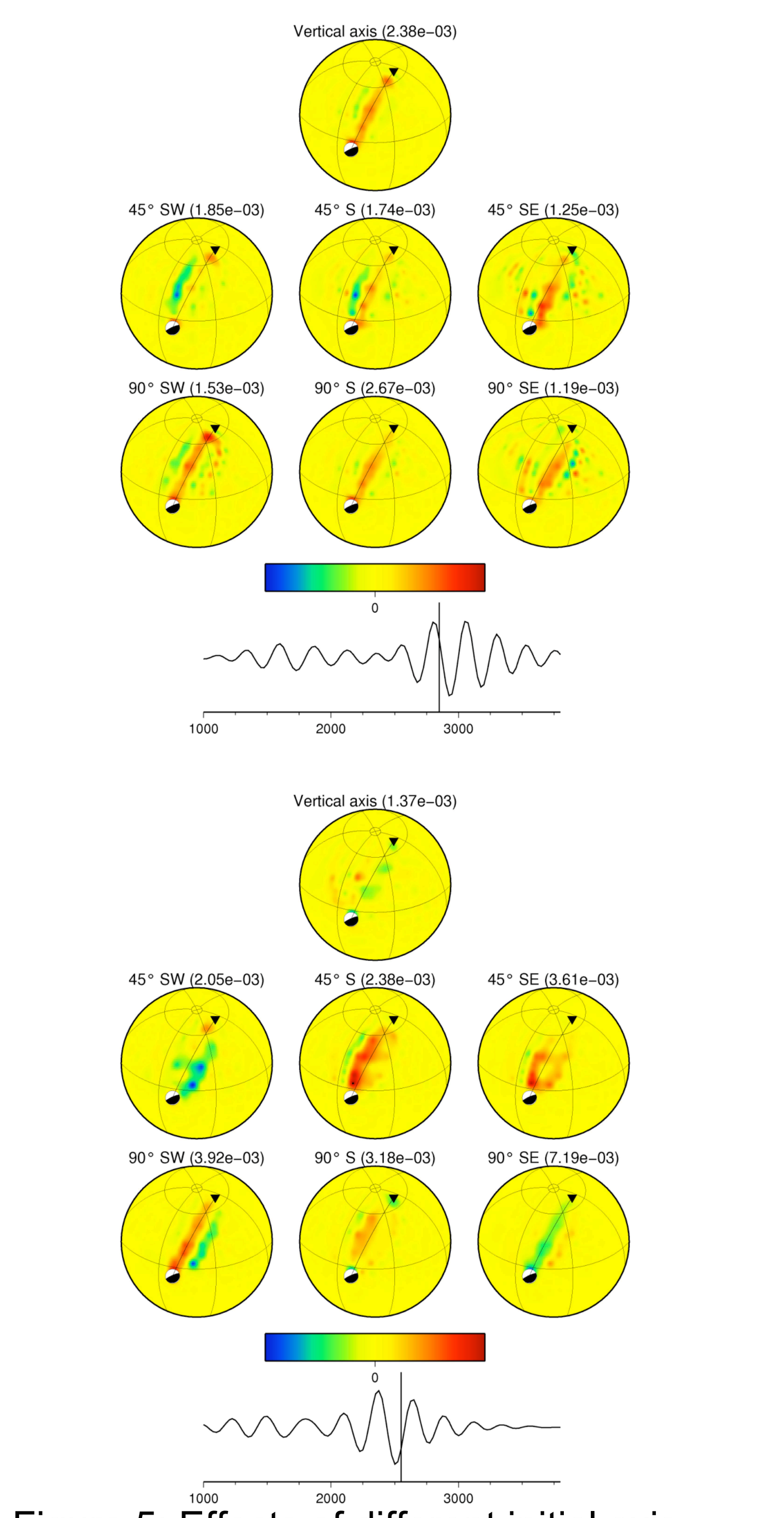

Figure 5: Effects of different initial axis orientation on Rayleigh (top) and Love (bottom) γ kernels. In each the top panel is the vertical axis kernel, while the lower panels show 45° tilt (middle) and horizontal axes (bottom), towards the SW (left), S (center), and SE (right).

Future modeling prospects

The parameterization chosen in this study is ideal for reducing the number of anisotropic parameters in a physically meaningful way. Both theoretical predictions (Becker et al. 2006) and observations of upper mantle xenoliths (Montagner and Anderson 1989) suggest that the 3 anisotropic parameters are highly correlated, and can then be scaled in an inversion. P and S perturbations can also be scaled, meaning we need only one isotropic and one anisotropic parameter, plus the two orientation angles.

Other parameterizations of general anisotropy (e.g. Montagner and Nataf 1986) are less suited to reducing the number of parameters, and numerical studies show that surface waves can be sensitive to many parameters (Sieminski et al 2007). Further study, however, is necessary to determine the best strategy for handling the non-linearity of the inversion for this parameterization.

This parameterization is also the same proposed in Chevrot (2006) for the inversion of SKS splitting intensity data using finite frequency kernels (figure 6). This suggests a potentially powerful joint inversion of these two complementary datasets in a consistent theoretical framework.

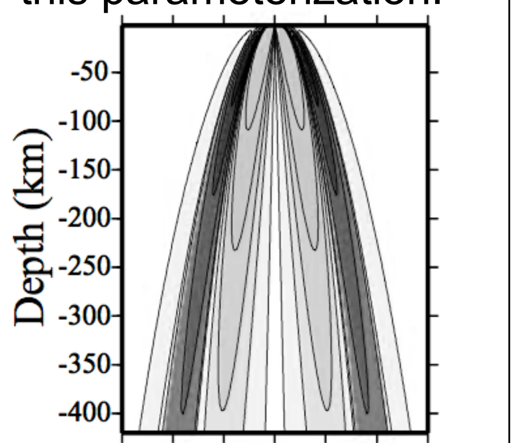

Figure 6: Example of a finite frequency SKS splitting intensity kernel (**from Favier and Chevrot 2003**)

References

Abt, D.L. and K.M. Fischer, 2007. "Resolving three-dimensional anisotropic structure with shear-wave splitting tomography," *Geophys. J. Int.*, in revision.

Becker, T.W., J.B. Kellogg, G. Ekström, and R.J. O'Connell, 2003. "Comparison of azimuthal seismic anisotropy from surface waves and finite strain from global mantle circulation models," *Geophys J. Int*. **155**, 696-714.

Becker, T.W., S. Chevrot, V. Schulte-Pelkum, and D.K. Blackman, 2006. "Statistical properties of seismic anisotropy predicted by upper mantle geodynamic models," *J. Geophys. Res*. **111**, doi:10.1029/2005JB004095.

Chevrot, S., 2006. "Finite-frequency vectorial tomography: a new method for high-resolution imaging of upper mantle anisotropy," *Geophys. J. Int*. **165**, 641-657.

Favier, N. and S. Chevrot, 2003. "Sensitivity kernels for shear wave splitting in transverse isotropic media," *Geophys. J. Int*. **153**, 213-228.

Mensch, T. and P. Rasolofosaon, 1997. "Elastic-wave velocities in anisotropic media of arbitrary symmetry - generalization of Thomsen's parameters ε, δ, and γ," *Geophys. J. Int.* **128**, 43-64.

Montagner, J.-P. and D.L. Anderson, 1989. "Petrological constraints on sesimic anisotropy," *Phys. Earth Planet. Inter*. **54**, 82-105.

Montagner, J.-P. and H.C. Nataf, 1986. "A simple method for inverting the azimuthal anisotropy of surface waves," *J. Geophys. Res*. **91**, 511-520.

Sieminski, A., Q. Liu, J. Trampert, and J. Tromp, 2007. "Finite-frequency sensitivity of surface waves to anisotropy based upon adjoint methods," *Geophys. J. Int*. **168**, 1153-1174.

Simons, F.J., R.D. van der Hilst, J.-P. Montagner, and A. Zielhuis, 2002. "Multimode Rayleigh wave inversion for heterogeneity and azimuthal anisotropy of the Australian upper mantle," *J. Geophys. Res*. **151**, 738-754.

Zhou, Y., F.A. Dahlen, and G. Nolet, 2004. "Three-dimensional sensitivity kernels for surface wave observables," *Geophys. J. Int*. **158**, 142-168.